Effect of Band Structure on Quantum Interference in Multiwall Carbon Nanotubes

Bernhard Stojetz,[1] Csilla Miko,[2] Laszlo Forró,[2] and Christoph Strunk[1]

[1]*Institute of Experimental and Applied Physics, University of Regensburg, 93040 Regensburg, Germany*

[2]*Institute of Physics of Complex Matter, FBS Swiss Federal Institute of Technology (EPFL), CH-1015 Lausanne, Switzerland*

(Received 28 October 2004; published 10 May 2005)

We report conductance measurements on multiwall carbon nanotubes in a perpendicular magnetic field. A gate electrode with large capacitance is used to considerably vary the nanotube Fermi level. This enables us to search for signatures of the unique electronic band structure of the nanotubes in the regime of diffusive quantum transport. We find an unusual quenching of the magnetoconductance and the zero bias anomaly in the differential conductance at certain gate voltages, which can be linked to the onset of quasi-one-dimensional subbands.

DOI: 10.1103/PhysRevLett.94.186802 PACS numbers: 73.63.Fg, 72.80.Rj

Quantum transport in multiwall carbon nanotubes (MWNT) has been intensely studied in recent years [1,2]. Despite some indications of ballistic transport even at room temperature [3,4], the majority of experiments revealed typical signatures of diffusive quantum transport in a magnetic field B such as weak localization (WL), universal conductance fluctuations (UCF), and the $h/2e$-periodic Altshuler-Aronov-Spivak (AAS) oscillations [2,5–7]. These phenomena are caused by the Aharonov-Bohm phase, either by coherent backscattering of pairs of time-reversed diffusion paths (WL and AAS) or by interference of different paths (UCF). In addition, zero bias anomalies caused by electron-electron interactions in the differential conductance have been observed [8]. The nanotubes have a very specific band structure consisting of many one-dimensional subbands with a spacing determined by the tube diameter [9]. For an undoped metallic tube, the Fermi level E_F is located at the charge neutrality point (CNP), where the bonding and antibonding π bands cross.

Hence, the question arises, how the band structure affects the quantum interference. In previous works the gates were weakly coupled, the induced shift of E_F being small compared to the subband spacing. In this experiment, we use a strongly coupled gate, which is efficient enough to shift the Fermi level through several quasi-one-dimensional subbands. At certain gate voltages, which can be associated with the bottoms of the subbands, we observe a strong suppression of both the magnetoconductance and the differential conductance.

The samples were produced on top of thermally oxidized Si wafers. First, Al strips of 10 μm width and 40 nm thickness were evaporated. Exposure to air provides an insulating native oxide layer of a few nm thickness. These strips serve as a back gate for the individual nanotubes, which are deposited from a chloroform suspension in the next step. Electric contacts are defined by electron beam lithography. After application of a gentle oxygen plasma, 80 nm of Au are deposited. In this way we achieve typical 2-point resistances between 10 kΩ and 30 kΩ at 4.2 K. The samples were operated by a low frequency ac voltage bias and application of a dc gate voltage U_{gate} to the Al layer. Up to gate voltages of 3 V no leakage current between the gate and the tube was observed ($I_{\mathrm{leak}} <$ 100 fA). Typical breakdown voltages of the gate oxide were 3–4 V. Two-terminal resistance measurements were carried out for two samples, A and B. The lengths of the samples are 5 μm and 2 μm and their diameters are 19 nm and 14 nm, respectively. A scanning electron micrograph of sample B is shown in Fig. 1(a).

Figure 1(b) shows the conductance G as a function of U_{gate} at 300 K. A shallow minimum in G(300 K) is located at $U_{\mathrm{gate}} \approx -0.2$ V. When the Fermi level E_F is tuned away from the CNP, higher subbands can contribute to the transport and an increase of the conductance is expected. Thus we attribute the position of the conductance minimum to the CNP, where states with energy $E > E_F$ are

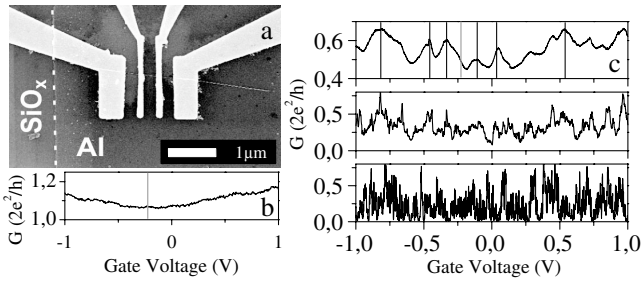

FIG. 1. (a) Scanning electron microscopy (SEM) image of sample B: individual MWNTs are deposited on a prestructured Al gate electrode and contacted by four Au fingers, which are deposited on top of the tube. The electrode spacing is 300 nm. Only the two inner electrodes are used. A second tube is located at the right outermost contact. (b) Conductance of sample A at 300 K as a function of gate voltage with an ac bias of 2 μV. The estimated position of the charge neutrality point (CNP) corresponds to the minimum of G and is indicated by the gray line. (c) Same as in Fig. 1(b), but for 10 K, 1 K, and 30 mK (top to bottom). For the 10 K curve, both the positions of the CNP (gray line) and the regions of quenched magnetoconductance (black lines) as observed in Fig. 2 are indicated.

unoccupied while those with $E < E_F$ are completely filled [10]. This reveals an n-doping of the tube, which is most probably induced by adsorbates on the tube. We observed p- as well as n-doping at $U_{\text{gate}} = 0$ V in different samples. The $G(U_{\text{gate}})$ curves in Fig. 1(c) show an increasing fluctuation amplitude as the temperature is lowered, while the average conductance decreases. This can be interpreted as a gradual transition from a coexistence of band structure effects and UCFs at 10 K and 1 K to the dominance of Coulomb blockade at 30 mK. In contrast to experiments on clean SWNT, no periodic Coulomb oscillations are found. Instead, irregular peaks in conductance occur. It is likely that the disorder induces a nonuniform series of strongly coupled quantum dots and that transport is governed by higher order tunneling processes [11]. In the following, we focus on results at higher temperature, where Coulomb blockade is negligible.

Next, conductance traces $G(U_{\text{gate}})$ were recorded at several temperatures and in magnetic fields perpendicular to the tube axis. The result at a temperature of 10 K is displayed as a color plot in Fig. 2(a). We have checked for several gate voltages that $G(B)$ is symmetric with respect to magnetic field reversal as required in a two point configuration (not shown). In addition, most of the curves show a conductance minimum at zero magnetic field. A closer look at the data reveals that both the amplitude and the width of the conductance dip vary strongly with gate voltage. In order to make this variation more visible, we subtracted $G(U_{\text{gate}})$ at $B = 0$ [see Fig. 1(c)] from all gate traces at finite fields. The deviation from the zero-field conductance is presented as a color plot in Fig. 2(b). The most striking observation is that the magnetoconductance (MC) disappears at certain gate voltages U^*, as indicated by arrows. These voltages U^* are grouped symmetrically around the conductance minimum at $U_{\text{gate}} \approx -0.2$ V in Fig. 1(b), which we have assigned to the CNP. The values of the CNP, as well as the values of U^*, have been indicated in Fig. 1(c) by gray and black vertical lines, respectively. The latter always coincide with conductance maxima. These observations lead us to the conjecture that the quenched MC may occur at the onset of subbands of the outermost nanotube shell, which for small contact spacing carries the major part of the current at low temperatures [7].

To confirm this idea, we applied a simple band structure model. The black line in Fig. 3(a) shows the density of states of a single wall (140, 140) armchair nanotube corresponding to the diameter of sample A (19 nm). Typical van Hove singularities indicate the positions of subband bottoms [9]. By integration over energy one obtains the number ΔN of excess electrons on the tube, plotted as a red line in Fig. 3(a). In this way, we can determine the number ΔN^* of excess electrons at the onset of the nanotube subbands. If we assume as usual a capacitative coupling between the gate and the tube, ΔN can be converted into a gate voltage via $CU_{\text{gate}} = e\Delta N$. In Fig. 3(b) the measured gate voltages U^* of quenched MC are plotted vs the calculated ΔN^* for both samples. Both data sets fit very well into straight lines,

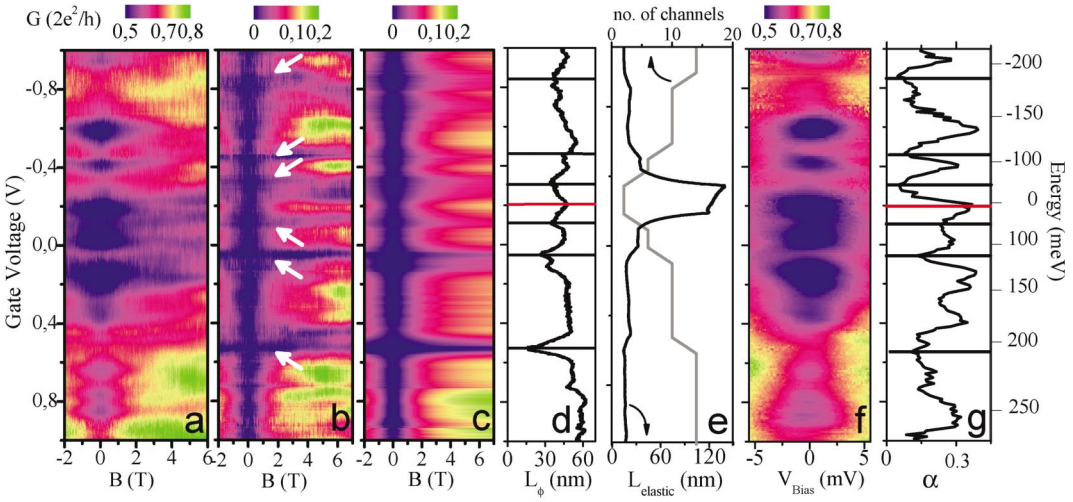

FIG. 2 (color). (a) Color coded conductance G of sample A as a function of gate voltage U and perpendicular magnetic field at a temperature of 10 K. (b) Color plot of the deviation of G from the zero-field conductance $G(U, B) - G(U, 0)$. White arrows indicate the regions of quenched magnetoconductance. (c) Reproduction of the magnetoconductance by 1D weak localization fits. The parameters L_φ and $G(B = 0)$ are used as obtained by fitting the data on Fig. 2(a). (d) Phase coherence length L_φ vs gate voltage as obtained from the fit. The positions of the charge neutrality point (red line) and the regions of quenched magnetoconductance (black lines) are indicated. (e) Elastic mean-free path (black) and number of transport channels per spin direction (gray) as a function of gate voltage. (f) Color coded differential conductance of sample A as a function of U and dc bias voltage V at $T = 10$ K. (g) Exponent α vs U as obtained from fitting a power law V^α to $G(U, V)$ in the range $eV \gg k_B T$. Right: scale conversion of the gate voltage into a (nonlinear) energy scale as described in the text.

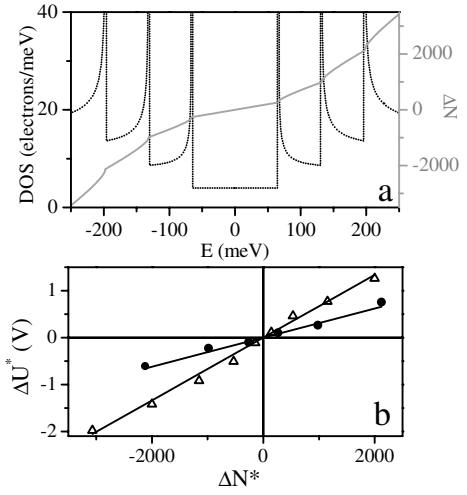

FIG. 3. (a) Calculated π-orbital DOS for a (140, 140) armchair nanotube of diameter of 19 nm (dotted) as a function of energy. Number of excess electrons $N(E)$ (gray) as obtained from the integration of the DOS from 0 to E. The subband spacing for this diameter is 66 meV. (b) Measured values U^* of quenched MC vs calculated numbers ΔN^* of electrons at subband onsets for sample A (circles, diameter 19 nm) and B (triangles, diameter 14 nm). The lines correspond to linear fits of the data. The slopes of the lines correspond to gate capacitances per length of 300 $a\mathrm{F}/\mu\mathrm{m}$ and 330 $a\mathrm{F}/\mu\mathrm{m}$ for samples A and B, respectively.

which demonstrates that most of the positions U^* of the quenched MC agree very well with the expected subband onsets. In addition, the gate capacitances C are provided by the slope of U^* vs ΔN^*. The capacitances per length are nearly identical, i.e., 300 $\mathrm{aF}/\mu\mathrm{m}$ and 330 $\mathrm{aF}/\mu\mathrm{m}$ for samples A and B, respectively. These values agree within a factor of 2 with simple geometrical estimates of C, indicating the consistency of the interpretation. From the capacitance C and the calculated dependence of the number of electrons N on energy, one can convert the gate voltage into an equivalent Fermi energy. This energy scale is shown at the right margin Fig. 2.

The typical dip in the MC at $B = 0$ in Fig. 2(a) has been observed earlier and can be explained in terms of weak localization (WL) in absence of spin-orbit scattering [2,6,12]. The WL correction ΔG_{WL} to conductance provides information on the phase coherence length L_φ of the electrons. With W being the measured diameter and $L = 300$ nm the contact spacing of the nanotube, ΔG_{WL} is given in the quasi-one-dimensional case ($L_\varphi > W$) by $\Delta G_{\mathrm{WL}} = -(e^2/\pi\hbar L)[L_\varphi^{-2} + (WeB)^2/3\hbar^2]^{-1/2}$. In Fig. 2(b) each row displays a dip at $B = 0$, where both the amplitude and the width of the dip vary strongly with gate voltage. We have used the WL expression above to fit the low field MC with L_φ and $G(B = 0)$ as free parameters. The conductance ΔG_{WL} as calculated using the fit parameters is plotted in Fig. 2(c). We find that the conductance traces are reproduced very well by the fit for fields up to 2 T. For higher fields, deviations occur, most probably due to residual UCF. In this way, we obtain an energy dependent $L_\varphi(E_{\mathrm{F}})$, which is plotted in Fig. 2(d). L_φ varies from 20 to 60 nm and displays clear minima which correspond to the regions of nearly flat MC in Fig. 2(b). From the preceding discussion, we can say that the WL seems to be suppressed at the onset of the nanotube subbands. To our knowledge, a theoretical explanation for this effect is not yet available.

In order to confirm the validity of our interpretation in terms of weak localization, we have studied the temperature dependence of the phase coherence length. As the dominating dephasing mechanism, quasielastic electron-electron scattering has been identified [2,6,13]. Dephasing by electron-phonon scattering is negligible since the corresponding mean-free path exceeds 1 μm even at 300 K [14,15]. The theory by Altshuler, Aronov, and Khmelnitzky [16] predicts $L_\varphi = (GDL\hbar^2/2e^2k_{\mathrm{B}}T)^{1/3}$, where $D = v_F L_{\mathrm{el}}/2$ the diffusion constant and L_{el} the elastic mean-free path. The dominance of electron-electron scattering can be confirmed by studying the temperature dependence of L_φ. Therefore, the MC measurements have been repeated for temperatures ranging from 1 K to 60 K. In order to eliminate the UCF contribution, the MC curves have been averaged over the whole range of U_{gate}. For an average L_{el} of the order $\sim$20 nm (see below), the Thouless energy E_C of the tube equals 70 μeV. Thus, the averaged range $\sim$400 meV is much larger than E_C. The result is plotted in Fig. 4(a). For the comparison of the curves with theory, one has to bear in mind that the average runs also on curves with suppressed MC. Hence, for the fit an averaged weak localization contribution of the form

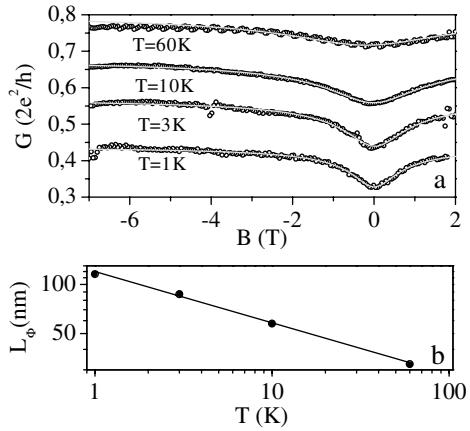

FIG. 4. (a) Averaged magnetoconductance of sample A (circles) at temperatures of 60 K, 10 K, 3 K, and 1 K (top to bottom) and fits of 1D weak localization behavior (lines) with scaling factors $A = 0.61$, 0.48, 0.35, and 0.22 (top to bottom) as described in the text. (b) Double-logarithmic plot of the temperature dependence of the phase coherence length L_φ as obtained from the weak localization fit (black dots). The line corresponds to a power law fit with an exponent -0.31.

$\Delta G^*_{\mathrm{WL}} = A\Delta G_{\mathrm{WL}}$ with a scaling factor $0 < A < 1$ has been taken into account. The fitted curves are included in Fig. 4(a). They match the data very well, up to magnetic fields of 7 T. In Fig. 4(b) the resulting average values of $L_\varphi(T)$ are shown. As expected, the contribution of the UCF is completely suppressed by the ensemble averaging. The temperature dependence matches a power law with exponent -0.31, which is close to the theoretical prediction of $-1/3$. From the abscissa of Fig. 4(b) we can also extract an average diffusion coefficient $\langle D \rangle$, which corresponds an average $\langle L_{\mathrm{el}} \rangle = 22$ nm.

Independent information about L_{el} can be obtained from the measured resistance of the sample, which in the regime $L > L_\varphi > L_{\mathrm{el}}$, is given by [17]: $R = R_C + h/2e^2[ML_{\mathrm{el}}/(L + L_{\mathrm{el}}) - L_\varphi/L]^{-1}$, where R is the 2-terminal resistance, M is the number of conducting channels per spin direction, and R_C is the contact resistance. $M(U_{\mathrm{gate}})$ is extracted from the subband assignment, where a finite slope at the band edges has been introduced by hand to account for disorder smearing. For R_C, a typical value of 2.5 kΩ was assumed. The results for $L_{\mathrm{el}}(U_{\mathrm{gate}})$ and $M(U_{\mathrm{gate}})$ are shown in Fig. 2(e). We find $L_{\mathrm{el}} \approx 130$ nm at the CNP and a rapid drop of the onsets of higher subbands, down to $\sim$20 nm. This can be understood in terms of a strongly enhanced scattering rate resulting from the opening of new scattering channels. Very similar results have been obtained for disordered SWNTs in the numerical calculations by Triozon *et al.* [18]. Averaging over all U_{gate} results in $\langle L_{\mathrm{el}} \rangle = 31$ nm, in reasonable agreement with the result of the T dependence of $\langle L_\varphi \rangle$. The behavior of L_{el} reflects the rather weak modulation of $G(U_{\mathrm{gate}})$ at 10 K [see Fig. 1(b)]. In the vicinity of the CNP L_{el} exceeds L_φ. Although one may expect modifications of the WL in this regime, these are not apparent in our data.

Another quantum correction to the conductance is induced by the electron-electron interaction and reduces the density of states near the Fermi energy [19]. This leads to zero bias anomalies (ZBA) in the differential conductance dI/dV [8], from which information on the strength of the electron-electron interaction can be extracted. In the case of tunneling into an interacting electron system with an Ohmic environment, the differential conductance dI/dV is given by a power law, i.e., $dI/dV \propto V^\alpha$ for $eV \gg k_{\mathrm{B}}T$, where the exponent α depends both on the interaction strength and the sample geometry [20]. In order to obtain complementary information, we have examined the dependence of the ZBA on the gate voltage U_{gate}. The differential conductance has been measured as a function of U_{gate} and V_{bias}. The result is presented in Fig. 2(f). For each gate voltage, the conductance shows a dip at zero bias. The zero bias anomaly has a strongly varying width with gate voltage and nearly vanishes at the same gate voltages $U_{\mathrm{gate}} = U^*$ as the magnetoconductance. For each value of the gate voltage, a power law fit for the bias voltage dependence of the differential conductance has been performed. The resulting exponent $\alpha(U_{\mathrm{gate}})$ is plotted in Fig. 2(g). α varies between 0.03 and 0.3 and shows again clear minima at the gate voltages U^*. A similar gate modulation of α has been observed by Kanda *et al.* [21], but was not related to the band structure. According to the theory [19], the energy dependence of α should be related to that of L_{el}. A further analysis of this relation requires an independent measurement of the density of states (DOS) and is beyond the scope of this Letter.

In conclusion, we observe experimentally a strong correlation between the single particle interference effects (expressed by L_φ) and the interaction effects (expressed by α). Both show clear minima at certain positions of the Fermi level, which match well the positions of the van Hove singularities estimated from simple band structure models.

We have benefitted from inspiring discussions with A. Bachtold, V. Bouchiat, G. Cuniberti, H. Grabert, M. Grifoni, K. Richter, S. Roche, R. Schäfer, C. Schönenberger, and F. Triozon. Funding by the Deutsche Forschungsgemeinschaft within the Graduiertenkolleg 638 is acknowledged. The work in Lausanne was supported by the Swiss National Science Foundation.

[1] C. Dekker, Phys. Today **52**, No. 5, 22 (1999).
[2] C. Schönenberger *et al.*, Appl. Phys. A **69**, 283 (1999).
[3] S. Frank *et al.*, Science **280**, 1744 (1998).
[4] A. Urbina *et al.*, Phys. Rev. Lett. **90**, 106603 (2003).
[5] L. Langer *et al.*, Phys. Rev. Lett. **76**, 479 (1996).
[6] K. Liu *et al.*, Phys. Rev. B **63**, 161404 (2001).
[7] A. Bachtold *et al.*, Nature (London) **397**, 673 (1999).
[8] A. Bachtold *et al.*, Phys. Rev. Lett. **87**, 166801 (2001).
[9] R. Saito *et al.*, J. Appl. Phys. **73**, 494 (1993).
[10] M. Krüger *et al.*, New J. Phys. **5**, 138 (2003).
[11] P. L. McEuen *et al.*, Phys. Rev. Lett. **83**, 5098 (1999).
[12] R. Tarkiainen *et al.*, Phys. Rev. B **64**, 195412 (2001).
[13] B. Stojetz *et al.*, New J. Phys. **6**, 27 (2004).
[14] J.-Y. Park *et al.*, Nano Lett. **4**, 517 (2004).
[15] A. Javey *et al.*, Phys. Rev. Lett. **92**, 106804 (2004).
[16] B. L. Altshuler, A. G. Aronov, and D. Khmelnitzkii, Solid State Commun. **39**, 619 (1981).
[17] S. Datta, *Electron Transport in Mesoscopic Systems* (Cambridge University Press, Cambridge, England, 1995).
[18] F. Triozon *et al.*, Phys. Rev. B **69**, 121410(R) (2004).
[19] R. Egger and A. O. Gogolin, Phys. Rev. Lett. **87**, 066401 (2001); E. G. Mishchenko, A. V. Andreev, and L. I. Glazman, Phys. Rev. Lett. **87**, 246801 (2001); J. Rollbühler and H. Grabert, Phys. Rev. Lett. **91**, 166402 (2003).
[20] C. L. Kane and M. P. A. Fisher, Phys. Rev. B **46**, 15233 (1992).
[21] A. Kanda *et al.*, Phys. Rev. Lett. **92**, 036801 (2004).